Searching for calcium-aluminum-rich inclusions in cometary particles with Rosetta/COSIMA

John Paquette, Cecile Engrand, Oliver Stenzel, Martin Hilchenbach, Jochen Kissel, The Cosima Team

The Meteoritical Society

Meteoritics & Planetary Science 51, Nr 7, 1340–1352 (2016)
doi: 10.1111/maps.12669

Searching for calcium-aluminum-rich inclusions in cometary particles with Rosetta/COSIMA

John A. PAQUETTE[1*], Cecile ENGRAND[2], Oliver STENZEL[1], Martin HILCHENBACH[1], Jochen KISSEL[1], and the COSIMA Team

[1]Max-Planck-Institut für Sonnensystemforschung, Justus-von-Liebig-Weg 3, 37077 Göttingen, Germany
[2]Centre de Sciences Nucléaires et de Sciences de la Matière—CSNSM, CNRS/IN2P3-Univ. Paris Sud (UMR8609), Université Paris-Saclay, Bat. 104, 91405 Orsay, France
[*]Corresponding author. E-mail: paquette@mps.mpg.de

(Received 08 December 2015; revision accepted 08 April 2016)

Abstract–The calcium-aluminum-rich inclusions (CAIs) found in chondritic meteorites are probably the oldest solar system solids, dating back to 4567.30 ± 0.16 million years ago. They are thought to have formed in the protosolar nebula within a few astronomical units of the Sun, and at a temperature of around 1300 K. The Stardust mission found evidence of CAI-like material in samples recovered from comet Wild 2. The appearance of CAIs in comets, which are thought to be formed at lower temperatures and larger distances from the Sun, is only explicable if some mechanism allows the efficient transfer of such objects from the inner solar nebula to the outer solar nebula. Such mechanisms have been proposed such as an X-wind or turbulence. In this work, particles collected from within the coma of comet 67P/Churyumov–Gerasimenko are examined for compositional evidence of the presence of CAIs. COSIMA (the Cometary Secondary Ion Mass Analyzer) uses secondary ion mass spectrometry to analyze the composition of cometary dust captured on metal targets. While CAIs can have a radius of centimeters, they are more typically a few hundred microns in size, and can be smaller than 1 μm, so it is conceivable that particles visible on COSIMA targets (ranging in size from about 10 μm to hundreds of microns) could contain CAIs. Using a peak fitting technique, the composition of a set of 13 particles was studied, looking for material rich in both calcium and aluminum. One such particle was found.

INTRODUCTION

Since their discovery in the late 1960s (Christophe Michel-Levy 1968), calcium-aluminum-rich inclusions (CAIs) found in chondritic meteorites have drawn a lot of attention. They are thought to be the oldest solar system solids, dating back to 4567.3 ± 0.16 million years ago (Connelly et al. 2012). While the largest CAIs can have diameters of a few centimeters, they are more typically a few hundred microns in size, and can be smaller than 1 μm (Greshake et al. 1996; MacPherson 2005; Charnoz et al. 2015). An example of a submillimeter-sized CAI found in an Antarctic micrometeorite is shown in Fig. 1. The inclusions indicated by the arrows are spinel ($MgAl_2O_4$), a refractory mineral typical of CAIs. As the scale bar in Fig. 1 shows, these inclusions are only a few microns across and about 10–20 μm long. CAIs are found in every type of chondritic meteorites except for CI meteorites that in turn contain a very small amount of anhydrous minerals. They are composed mainly of oxides and silicates of calcium, aluminum, magnesium, and titanium (MacPherson 2005). As CAIs are enriched in refractory elements and rich in ^{16}O, they are probably formed in the protosolar nebula close to the Sun, and at a temperature of around 1300 K (Connelly et al. 2012). Because comets are formed beyond the snow line, at much lower temperatures, an absence of CAIs might be expected in cometary material, but the Stardust mission found evidence of CAI-like material in samples recovered from comet Wild 2 (Brownlee et al. 2006; Zolensky et al. 2006;

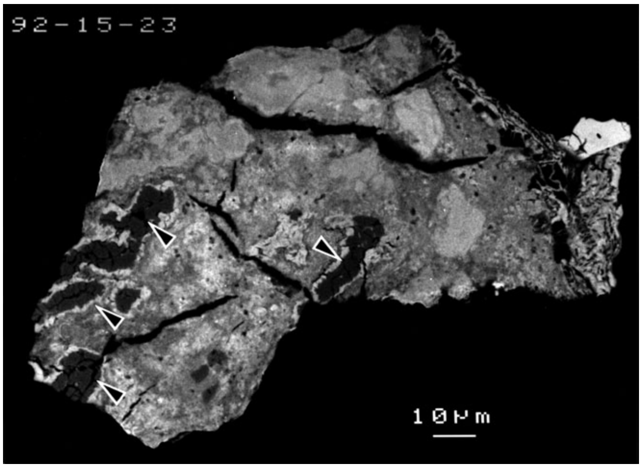

Fig. 1. Small calcium-aluminum-rich inclusions in an Antarctic micrometeorite collected at Cap Prudhomme. The inclusions indicated by the arrow consist of spinel ($MgAl_2O_4$), a refractory mineral typical of CAIs, with tiny perovskite inclusions ($CaTiO_3$). The spinel inclusions are surrounded by rims of Fe-rich dehydrated phyllosilicates. As the scale bar shows, these inclusions are only a few microns across and roughly 10–20 μm in length.

Simon et al. 2008; Schmitz et al. 2009; Matzel et al. 2010; Joswiak et al. 2013).

In this work, particles collected from within the coma of comet 67P/Churyumov–Gerasimenko by the dust instrument COSIMA are examined for evidence of CAIs using time-of-flight secondary ion mass spectrometry. Given the minimum observed size for CAIs in meteorites and micrometeorites, it is possible that particles visible on COSIMA targets (ranging in size from about 10 μm to hundreds of microns) could contain CAIs. COSIMA being a mass spectrometer, no information on mineralogy can be recovered directly; however, a compositional signature in the form of calcium and aluminum enrichments has been sought.

SAMPLES AND METHODS

The COSIMA Instrument

COSIMA is an instrument aboard the Rosetta spacecraft, which is designed to capture, image, and determine the composition of cometary dust particles. Twenty-four target holders, each with three 1 cm by 1 cm targets, are kept in storage when not in use. Targets are covered with gold, silver, palladium, or platinum. A target manipulator unit (TMU) moves a target holder in front of a dust funnel so that cometary dust entering the instrument can strike the target and adhere to it. The TMU can then move the target holder in front of COSISCOPE (an internal camera) to be imaged, and then into the path of a beam of 8 keV positive indium ions for time-of-flight secondary ion mass spectrometry (ToF-SIMS). The indium beam pulses have 3 ns duration and a 1.5 kHz repetition rate. The primary indium ions from the beam eject secondary ions from dust particles on the target, which are directed into a reflectron time-of-flight mass spectrometer. Precise measurement of the time-of-flight allows a precise measurement of the mass per charge of secondary ions. As most of such ions carry one unit of electric charge, this technique often directly yields the mass of the secondary ions. Thus, a mass spectrum of secondary ions is produced, providing composition information on a cometary dust particle. The potential can be set to collect either negative or positive secondary ions. In this work, only the spectra of positive secondary ions are considered, as rock-forming elements preferentially form positive secondary ions in these conditions. While the ion beam does not penetrate more than a few atomic layers into a particle, dust particles are typically crushed on impact, and portions of particles—sometimes quite substantial portions—have been observed to be removed during SIMS. Thus, the composition measured by COSIMA is not solely that of any surface film, but is indicative of the dust particle interior as well. Target holders can also be heated at the chemical station to reduce contamination if desired. A more complete description of COSIMA is available in Kissel et al. (2007).

Particles Collected by COSIMA from Comet 67P/ Churyumov–Gerasimenko

Rosetta reached comet 67P/Churyumov–Gerasimenko in August 2014. COSIMA began collecting cometary dust shortly after that. Previous missions to comets (such as Giotto and Stardust) were cometary flybys, with a relatively short duration close to the nucleus and a large relative velocity of measured dust particles. Rosetta is not a flyby mission. Instead it remains within a few tens to a few hundreds of kilometers of the nucleus of 67P/Churyumov–Gerasimenko, thus the relative velocity of arriving cometary dust particles is low—of the order of meters per second (Rotundi et al. 2015). Thus, the particles collected by COSIMA are relatively unaltered in composition (aside from the loss of volatiles; as the temperature of COSIMA is 10–15 °C, ices not lost in transit will not remain for long after they are collected).

The particles that have been observed by COSIMA have a range of sizes (Langevin et al. 2016; Merouane et al. 2016). Particles smaller than about 10 μm cannot be imaged by COSISCOPE (which has a 14 μm pixel size). This sets the minimum detectable size. The largest particles that have so far been collected are up to

Table 1. Dust particles analyzed.

Particle name	Target	Collection period	Mean solar distance (AU)	Median cometocentric distance (km)
Alina Peruvesi	3D0	August 2014	3.18 ± 0.02	11
Anais Enovesi	2D0	August 2014	3.51 ± 0.02	73
Boris Enovesi	1D0	August 2014	3.51 ± 0.02	73
David Toisvesi.2	2D1	May 2015	1.66 ± 0.002	154
Donia Enovesi	2D0	August 2014	3.51 ± 0.02	73
Felix Jonkeri	3D0	September 2014	3.40 ± 0.02	30
Francois Enovesi	1D0	August 2014	3.51 ± 0.02	73
Hanna Hankavesi	1D0	August 2014	3.48 ± 0.01	56
Johannes Peruvesi	3D0	August 2014	3.18 ± 0.02	11
Kathrin Enovesi	3D0	August 2014	3.51 ± 0.02	73
Nicolas Ala-Kitka	2D0	August 2014	3.55 ± 0.02	97
Oskar Enovesi	1D0	August 2014	3.51 ± 0.02	73
Roberto Toisvesi.1	2D1	May 2015	1.66 ± 0.002	138

800 μm across. COSIMA particles are given names for ease of reference. The first name identifies the individual particle, the second name the week of its collection, and (for targets imaged more than once per week) a number may be appended indicating when during that week the particle was collected. More information about the operation of COSISCOPE is available in Kissel et al. (2007) and in Langevin et al. (2016). The size distribution, flux, and morphological classification of the dust are described in Langevin et al. (2016) and Merouane et al. (2016). While, as of December 2015 over 10,000 particles have been collected, only a small fraction has thus far been subjected to secondary ion mass spectrometry. The particles which will be discussed in this paper were captured on four gold targets (designated 1D0, 2D0, 3D0, and 2D1), all of which were coated with gold black, formed by the evaporation of gold in a low pressure argon atmosphere (Hornung et al. 2014). This work will be limited to 13 of the particles that have been analyzed using SIMS. These 13 particles are listed in Table 1.

As Fig. 2 illustrates, SIMS is generally performed using a matrix scan (with the location on the target of the center of the ion beam varying in a regular pattern over the target; see Fig. 2a) or a line scan in which one coordinate is fixed and the other is varied by regular steps (as shown in Fig. 2b). The reason for this is that hitting a particle with the ion beam requires fine positioning of the target and beam. Striking the desired particle is achieved through scanning the target in front of the primary ion beam. The spectra taken off of the particle are used as local background to remove the possible contribution of the target signal on the spectra of the particle, if the size of the particle is smaller than that of the ion beam. There can be some shift between the positions of the ion beam in the acquisition of positive or negative secondary ions. This shift is compensated by the input of apparent different coordinates between the two modes. In particular, in Fig. 2, the target is shifted along the y-axis so that the negative and positive spectra will be in fact be taken at the same locations.

RESULTS

Figure 3 illustrates some results from the line scan across particle David Toisvesi.2 that was shown in Fig. 2b. In Fig. 3, the ratio of sodium to hydrogen and the ratio of magnesium to hydrogen are plotted versus the X coordinate of the target. The locations which show high sodium and magnesium signals are taken to be on the particle, as these two species are absent or present at very low levels on the target substrate, and have been seen in cometary dust particles gathered by COSIMA (Schulz et al. 2015). The ratio of elements to hydrogen is used to eliminate any effect from variability in the indium beam with time, or variation in secondary ion yields between the particle and the target. Hydrogen was used because it showed only a small variation over the scan. Spectra that show low elemental Na^+/H^+ and Mg^+/H^+ ratios can be of use as background measurements as described below. Alternatively, a decrease in ions believed to originate from the target substrate (such as Au on gold targets or various contaminants known to be on the target) may be used to identify spectra that are on the cometary particle.

A section of a mass spectrum resulting from one location on the line scan across David Toisvesi.2 is shown in Fig. 4a. The full mass spectrum spans the range from 1 to 3500 u with a mass resolution of $m/\Delta m > 1000$, but the section shown in Fig. 4a covers the mass range 1–200, with a few of the taller single peaks labeled. A full spectrum is produced at each location in the scans described above. Figure 4b shows

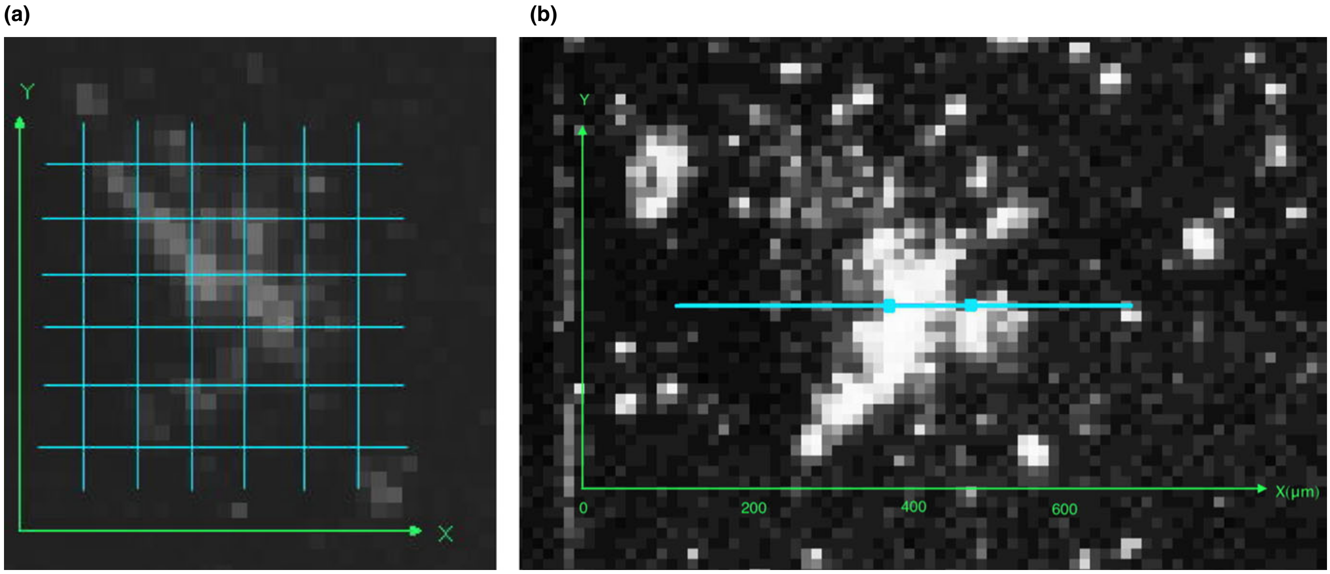

Fig. 2. In COSIMA, secondary ion mass spectrometry is generally performed using either a matrix scan or a line scan. a) A matrix scan around particle Hanna Hankavesi on target 1D0. It should be noted that particles on COSIMA targets are assigned names for ease of reference, with the first name distinguishing the individual particle and the second name the week of collection. If a target is imaged more than once in a week, a number may be appended. A COSISCOPE image of a section of target around the particle has superimposed on it a blue grid whose intersections are approximately the locations at which spectra were taken. The coordinate axes are shown in green. The particle is the light-colored area near the center of the image. The X (horizontal on the page) and Y (vertical on the page) coordinates of the ion beam on the target surface are varied in a regular pattern. Pixel size is 14 μm. b) A line scan that passes over particle David Toisvesi.2 on target 2D1. A COSCISCOPE image of a target section has a blue line superimposed on it showing the location of a line scan, with green lines for the axes, as above. One coordinate (Y in this case) is fixed and the other is varied in regular steps. The particle here is large and its shape is rather complex. Because a shift is possible between target and beam coordinates, the locations shown for spectra are an approximation, accurate within 20 μm.

a smaller section of the spectrum around mass 23, showing the measured data (points) together with a fit (dotted line). More than one peak is seen in the vicinity of some integer masses as can be seen in Fig. 4c. Often there will be an elemental peak (for ^{56}Fe in this case) and second peak at a slightly higher mass corresponding to an organic molecular ion. The peaks in the spectrum are fit using a Levenberg–Marquardt algorithm, with peak location and amplitude as fitting parameters. Peak shape can vary depending on instrument status. In the plots shown in Fig. 4, the peak shapes are fit as a double Gaussian with a constant separation (in time-of-flight) and a relative amplitude which is another fitting parameter. All peaks at a given integer mass are required to have the same shape, which is an artificial restriction to keep the number of fitting parameters down. Fitting allows close-lying peaks to be deconvoluted, and produces an integral of the counts in a peak rather than merely an amplitude, thus providing better statistics.

Because the COSIMA ion beam makes a spot on the target approximately 35 × 50 μm across (full width at half maximum), and because many particles are fluffy rather than compact, it is almost invariably the case that secondary ion signal seen at any location on a particle will have a contribution from the target substrate as well as from the particle. To correct for this, and remove the contribution from the substrate, a background subtraction must be performed. This can either be a general background taken from a number of spectra measured in areas of the target that are devoid of visible particles, or a spectrum taken near a particle which is very low in sodium and magnesium or showing high peaks known to be associated with the target. After normalizing both particle spectra and background spectra to their respective hydrogen counts, the background values are subtracted from those measured on the particle to give a net contribution. For example, for sodium:

$$Na_{\text{Net}} = Na_{\text{Particle}} - Na_{\text{Background}}\left(\frac{H_{\text{Particle}}}{H_{\text{Background}}}\right)$$

Figure 5 shows sections of the spectra near masses 27 and 40 for three different locations on the line scan depicted in Fig. 1b. In Figs. 5a and 5b, data from the location $X = 445$ is shown. This spectrum was chosen

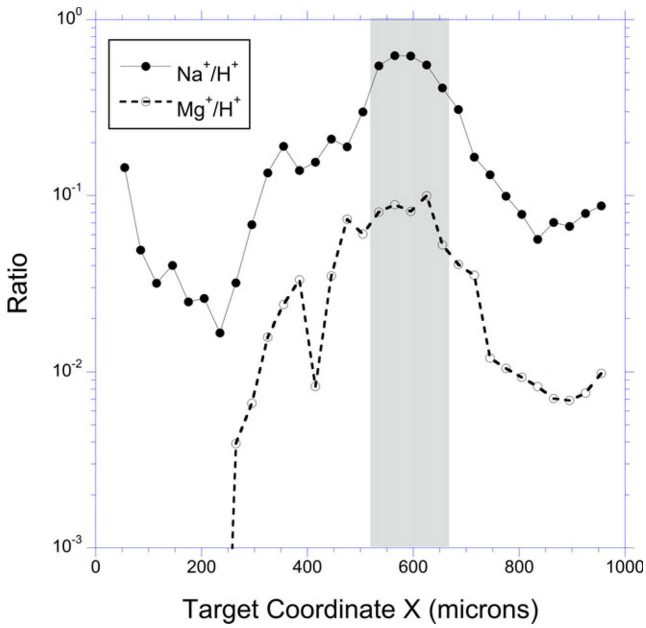

Fig. 3. Results from a line scan on the dust particle named David Toisvesi.2 which is shown in Fig. 2b. The ratios of sodium ions to hydrogen ions (solid circles, solid line) and magnesium ions to hydrogen ions (open circles, thicker dashed line) are plotted versus the target X coordinate (in microns). The increase in both ratios indicates that the spectrum from which they were taken is primarily from a dust particle rather than from the target substrate, as Na and Mg are not observed on the gold substrate, and have been seen in cometary dust particles gathered by COSIMA (Schulz et al. 2015). The ratio to hydrogen is used to eliminate any effect from variability in the indium beam with time, or in ionization yields between substrate and particle. Spectra taken as being on the particle are shown within a gray box. The ratios plotted here and in the following figures are atomic ratios.

because it is low in both sodium and magnesium, and thus is useful as a measurement of local background, that is, of contributions from the substrate rather than the particle David Toisvesi.2. In Fig. 5a, a peak is visible at mass 27.022 but none near 26.981, which is the expected location for an aluminum peak (as shown by a gray vertical line). This peak corresponds to an organic molecule (C_2H_3, whose expected location is shown by another gray vertical line) which is commonly observed in surfaces analyzed by ToF-SIMS, and therefore is associated to the target rather than with the cometary particle. Similarly, in Fig. 5b, a peak is visible near mass 40.031 but none at 39.962, where one would expect to find ^{40}Ca (as shown by a gray vertical line). Again, the peak at 40.031 is due to an organic molecule (C_3H_4, whose expected location is shown by another gray vertical line) and is again associated to surface contamination rather than being of cometary origin. We consider this spectrum to have little contribution from any cometary particles, instead it serves as a measure of the signal from the target substrate and is used as background.

Contrast this with the data shown in Figs. 5c and 5d, which is from location $X = 565$. This spectrum has much more sodium and magnesium than the previous one, and is thus considered to be on the particle (although still with some contribution from the target substrate). In Fig. 5c, the spectrum in the vicinity of mass 27 is plotted. At this time, some aluminum is visible (together with the peak at 27.022, as before). Figure 5d shows the vicinity of mass 40, highlighting a peak that is likely calcium in addition to the 40.031 C_3H_4 peak. In fact this spectrum also contains peaks corresponding to iron and nickel near masses 56 and 58. It may be noted that the aluminum peak is slightly to the left of the expected location, while the C_2H_3 peak is not. The effect is also visible for calcium, to a lesser degree. While the mass scale is quite accurate, a small shift of 1 or 2 channels may remain, but this would affect both peaks at a given mass equally. With the low counting rates involved, deriving a peak's mass accurately becomes more difficult—but it has been observed that peaks originating from a particle are sometimes found 1 or 2 time-of-flight channels to the left of the expected location, an effect not commonly seen in peaks originating from the target substrate. This can be due to the elevation of the particle with regard to the target, leading the ions from the cometary particles to have a smaller distance to travel and thus to arrive slightly earlier than those from the background. The elevation of the particle may not be the whole explanation of the effect; alteration of the extraction electric field by the particle may also play a role.

Finally, consider the data shown in Figs. 5e and 5f, which is from $X = 655$ in the same line scan. Here, a larger peak is visible at the location where aluminum is to be expected, and there is also a larger peak at the mass of ^{40}Ca, in addition to the ubiquitous organic peaks. This spectrum also has peaks at masses of manganese and iron (see Fig. 4c). The close-lying negative spectra (see the blue circles in Fig. 2b) showed no signature of any aluminum or calcium oxides but this may well be explained by the low counting rates and relative efficiencies involved.

After correction for instrumental relative sensitivity factors (Krüger et al. 2015), the atomic ratios of sodium, magnesium, aluminum, potassium, calcium, manganese, iron, and nickel are shown for several locations on particle David Toisvesi.2 in Fig. 6 and in Table 2. In the plot, the elements are shown normalized to iron and to the values seen in CI chondrites (representative of solar system abundances—taken from Lodders 2010). Location 655 shows an elevation in both calcium and aluminum as compared to the other

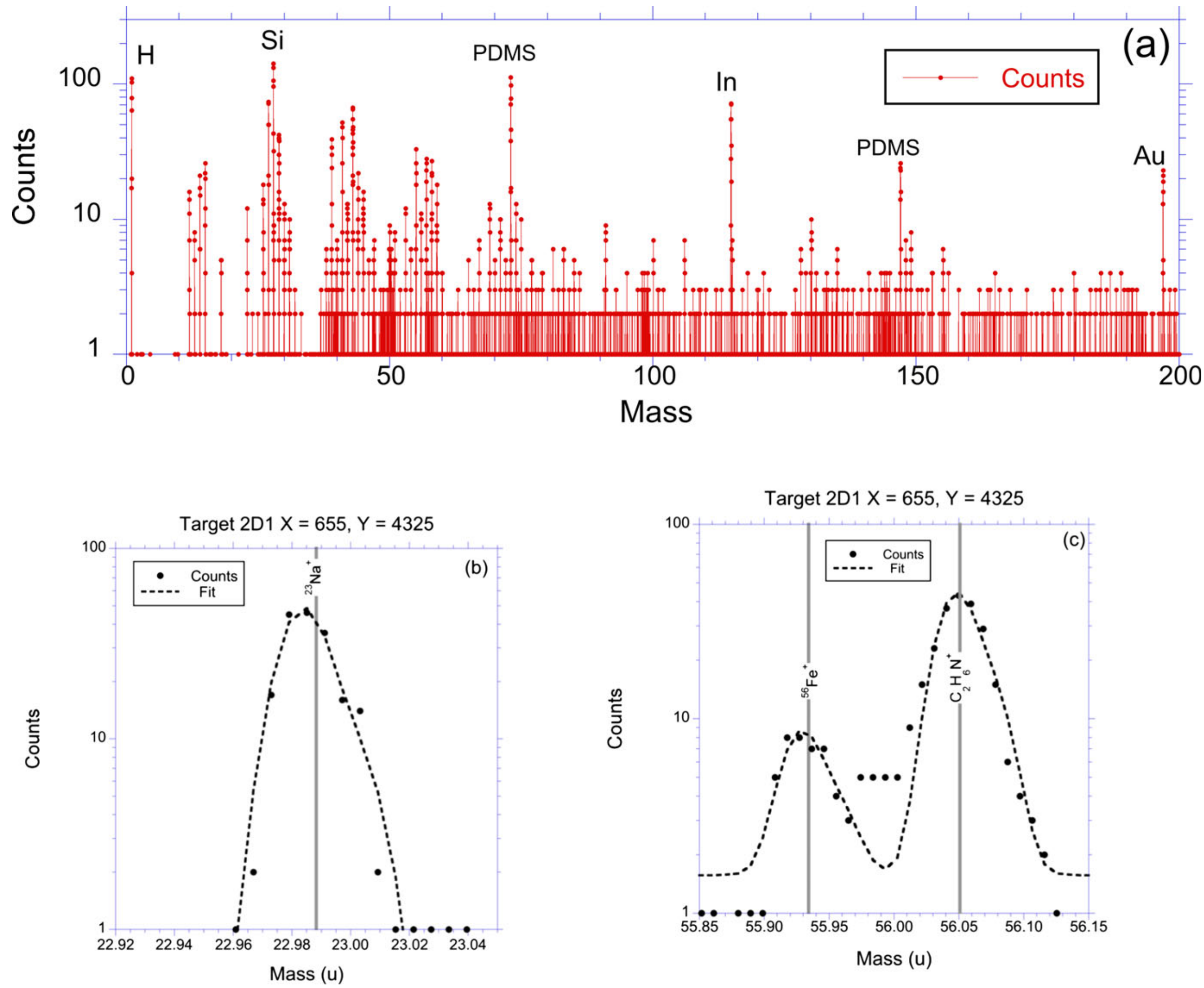

Fig. 4. a) A section of a COSIMA mass spectrum from mass 0 to 200, with a few of the taller single peaks labeled. Indium comes from the beam, gold comes from the substrate (as this spectrum was taken on a gold target), and PDMS refers to fragments of polydimethylsiloxane, a contaminant on some targets. A subsection of the spectrum from the vicinity of mass 23 is plotted in (b). The points in this panel are the data, the curve is a fit, and the gray vertical line indicates the expected location of sodium. c) Another subsection of the spectrum, this time in the neighborhood of mass 56. Again, the points are data, the curve is a fit, and the gray vertical lines indicate the masses of ^{56}Fe and C_2H_6N.

spectra, which are also on the particle as shown by the high sodium and magnesium values. Note that there is no net silicon signal (once the contribution from the target has been removed by the method described above) detectable from the particle. The Mn/Fe ratio is 20–70 times CI values and has been checked for interferences. Although manganese-rich olivines have been observed in close proximity with CAIs (Weisberg et al. 2004) and have also been detected in the Stardust data (Zolensky et al. 2006; Nakamura et al. 2008), the absence of a silicon signal from the particle casts doubt on the presence of these or any silicates in this particle.

Another particle on target 2D1, "Roberto Toisvesi.1" (depicted in Fig. 7), was analyzed with two intersecting line scans, but it had to be treated differently than particle David Toisvesi.2. The technique described above, of looking for spectra high in both sodium and magnesium to identify which spectra originated from the particle could not be used, as magnesium was very low or absent for all spectra in the line scan, while sodium was high for only a single location (X = 475), as shown in Fig. 8. That figure also shows that the contamination at mass 73 (caused by a fragment of polydimethylsiloxane (PDMS) a

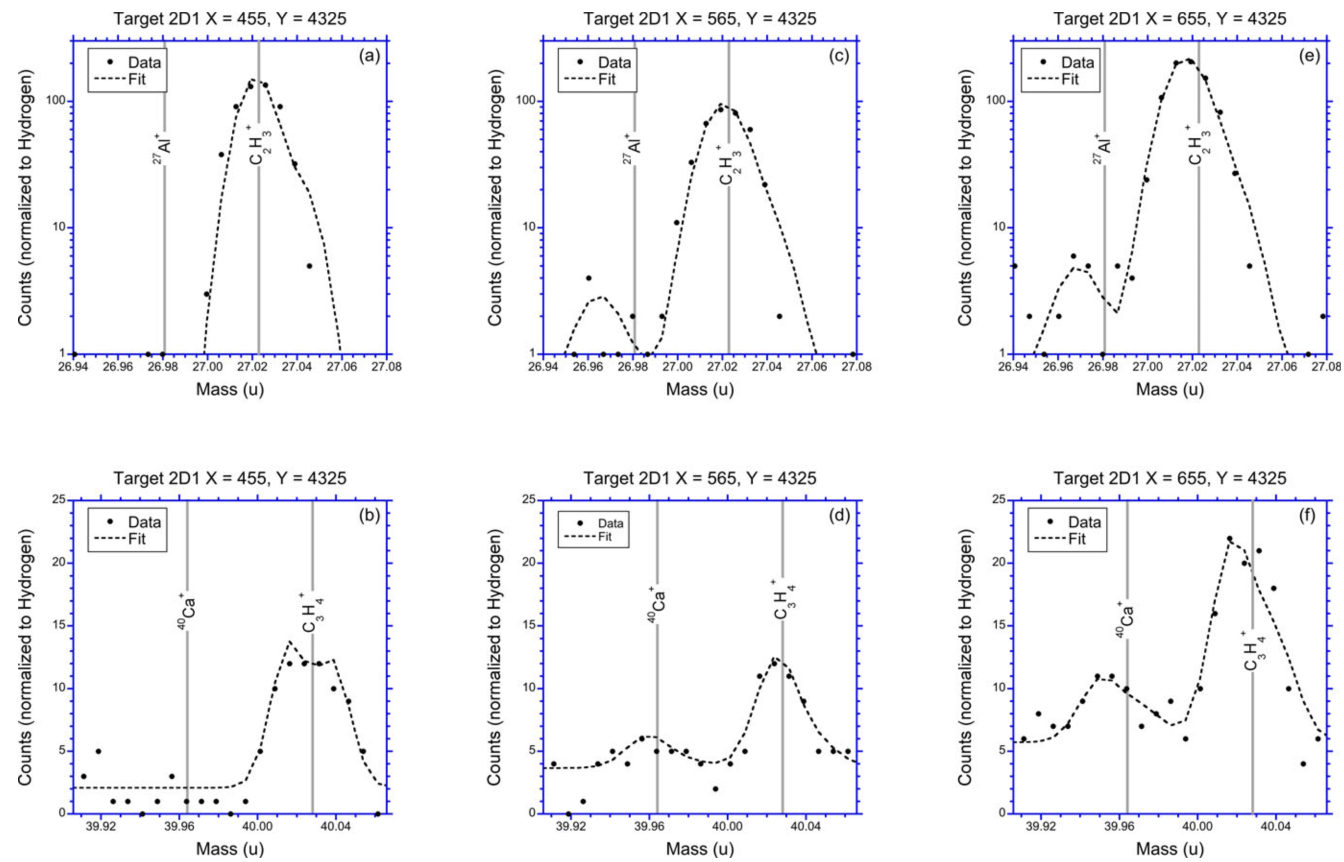

Fig. 5. Sections of COSIMA mass spectra from three different locations along a line scan across particle David Toisvesi.2. In all panels, the points are the measured counts (normalized to hydrogen at the same location, see the Results section of the text); the dotted curve is a fit to the data; and the gray vertical lines indicate the masses where aluminum, calcium, or organic peaks should show up if present at the indicated location. The three columns correspond to three locations on the target. The upper row of plots covers the vicinity of mass 27, the lower row the vicinity of mass 40. In (a) and (b) (corresponding to an X coordinate of 455 on the target), neither aluminum nor calcium is visible. In (c) and (d), small peaks are visible corresponding to both elements. In (e) and (f), those peaks are larger. The tendency for the aluminum and calcium peaks to lie to the left of where they might be expected has been observed in COSIMA positive spectra and may be an indicator of peaks coming from the particle rather than from the target.

contaminant seen on some COSIMA targets) shows no decrease, nor does gold, at $X = 475$. A possible explanation for this is that the signal at this location is from a small particle that is rich in calcium and aluminum, but is practically devoid of magnesium; there are several possible candidates. The gold and contamination ratios do not decrease much due to the particle's small size; most of the beam strikes the target even when the beam is on the particle, this implies a relatively small particle.

Based on the lower Na/H values and the large amounts of PDMS and gold, the spectrum at $X = 385$ was chosen as a background spectrum. The result of background subtraction is shown in Fig. 9 and in Table 3. The composition of Roberto Toisvesi.1 contains silicon, aluminum, potassium, calcium, and manganese, but it has neither iron nor magnesium. A small and approximately equivalent amount of iron is present in both the particle and the background spectra, so that in the net results no Fe remains. A possible explanation is that the weak iron signal observed in both spectra comes from small particles in the vicinity, while the high sodium, aluminum, and calcium signal comes from a small particle that is deficient in both Mg and Fe. As Fig. 9 shows, Roberto's abundances of calcium and aluminum are both somewhat lower than the corresponding CI chondrite values. It is possible that the abundance of Si (which was used to normalize) might be inflated due to an incomplete removal of the silicon arising from PDMS. This would artificially lower the Ca and Al abundances—in fact all the Si-normalized abundances—as illustrated in Fig. 9. Because we selected reference spectra with similar amounts of PDMS as the flight data, we are confident that the general effect of PDMS contamination is small with regard to our calibration method. Thus, available

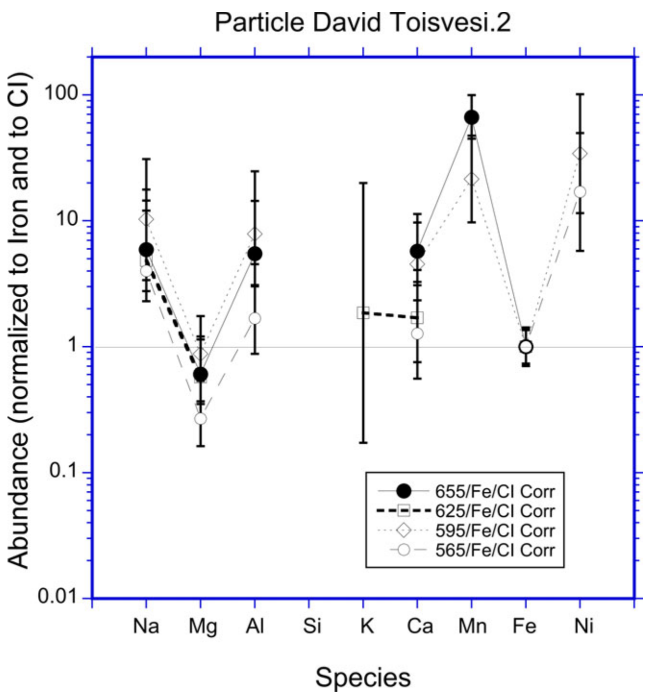

Fig. 6. Abundances normalized to iron and to CI chondrites for four locations on the particle David Toisvesi.2. Sodium, magnesium, calcium, and iron are seen at all four locations. Aluminum is not detected at $X = 625$ but potassium is. Mn is seen at $X = 595$ and $X = 655$ (and is quite high) and nickel is only detected at $X = 565$ and $X = 595$ (and is quite high). Silicon is not seen in any of the locations. Within the error bars, aluminum and calcium are consistent with the solar system value for location $X = 565$, but both are high for locations $X = 655$ and $X = 595$.

evidence does not support the conclusion that this particle is a CAI.

A similar analysis was carried out for particles Alina, Anais, Boris, Donia, Felix, Francois, Hanna, Johannes, Kathrin, Nicolas, and Oscar on targets 1D0, 2D0, and 3D0. For these particles, matrix scans rather than line scans were used. If spectra were available from the same scan which was low in magnesium and sodium or high in contamination, these were used as background. If that was not the case, background was taken from a number of SIMS spectra taken far from any visible dust particles. As the contamination on the target varies with time, the spectra chosen for the background were required to be relatively close in time (although not in space; location on the target was quite variable) to the measurements on the corresponding particles. Due to the presence of a larger signal from PDMS, a PDMS fragment at mass 73 was used for normalization and background subtraction rather than hydrogen. As can be seen from Fig. 10 and in Table 4, aluminum is not detected on any of the D0 particles except Kathrin, and only Anais, Donia, and Kathrin have any detectable level of calcium. These measurements were made in the late summer and early fall of 2014, and instrumental difficulties resulted in wider and more complex peak shapes. This was eventually improved by adjustment of instrument voltages, but the data are more difficult to fit than recent spectra. Because of this instrumental effect, the nondetection of calcium and aluminum in these dust particles does not rule out the presence of these elements at a low level. The high silicon abundances may reflect a contribution from PDMS as well as from the particle. Oscar is not plotted in Fig. 10, as no signal was seen from it except sodium and silicon. These particles are discussed in detail in Hilchenbach et al. 2016, but it can be seen from Fig. 10 that they fall into three distinct classes. Boris, Donia, Felix, Francois, Hanna, Johannes, and Nicolas are grouped close to the (Mg+Fe)/Si vertex and constitute one class. Anais is the richest in calcium but contains little aluminum, and Kathrin is unique among the D0 particles in containing both calcium and aluminum.

Donia's calcium abundance is in good agreement with that seen in CI chondrites. Kathrin has a high level of manganese as well as aluminum and calcium above CI chondrite levels, as well as sodium, magnesium, and silicon. The magnesium values may be depressed and the silicon values may be elevated by the effect of contamination (the presence of PDMS reduces the secondary ion yield for magnesium, and the contribution from the silicon in PDMS adds to silicon from the actual particle).

DISCUSSION

Comet 67P/Churyumov–Gerasimenko is a Jupiter-family comet, thought to have formed in the vicinity of Jupiter at relatively low temperatures. Thus, the comet should be largely composed of unprocessed and even primordial material (Levison and Morbidelli 2003). The appearance of CAIs (formed close to the protosun at high temperature) in comets is only explicable if some mechanism allows the efficient transfer of such objects from the inner solar nebula to the outer solar nebula—against the direction of the inward flow caused by gravitational collapse. Such mechanisms have been proposed such as an *X*-wind (Shu et al. 1996; Simon et al. 2008) or turbulence (Bockelee-Morvan et al. 2002; Ciesla 2007).

Nine of the dust particles analyzed by COSIMA show no detection of either calcium or aluminum. The analyses of particles on the D0 target holder present certain instrumental challenges, so the presence of calcium and aluminum at low levels is not ruled out by these measurements. The particle Donia contains

Table 2. Atomic ratios for locations in the scan across David Toisvesi.2.

X (microns)	Na/Fe	Mg/Fe	Al/Fe	Si/Fe	K/Fe	Ca/Fe	Mn/Fe	Ni/Fe
535	0.15	0.58	0.00	0.00	0.00	0.00	0.00	2.83
565	0.27	0.32	0.16	0.00	0.00	0.09	0.00	0.94
595	0.69	1.04	0.75	0.00	0.00	0.31	0.23	1.90
625	0.32	0.68	0.00	0.00	0.01	0.12	0.00	0.00
655	0.39	0.72	0.52	0.00	0.00	0.40	0.70	0.00

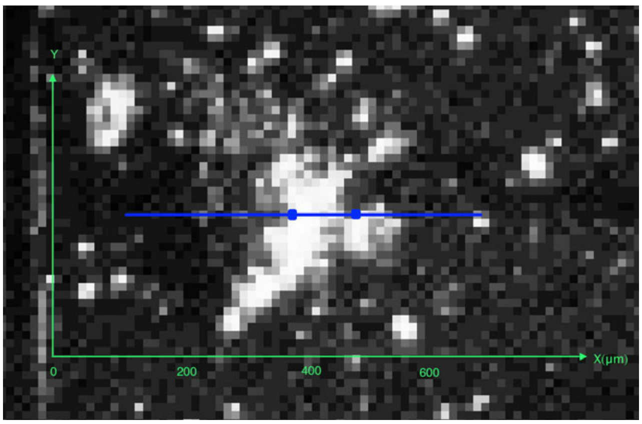

Fig. 7. SIMS measurements on particle Roberto Toisvesi.1 on target 2D1 consisted of two intersecting line scans. As in Fig. 2, the blue line denotes the location of a line scan across the particle, with spectra taken at 30 μm intervals and the pixel size is 14 μm. The blue squares indicate locations where spectra were chosen for analysis (either as background or as on the particle). The coordinate axes are shown in green. The particle Roberto is the light-colored area near the center of the image but numerous smaller particles are also present.

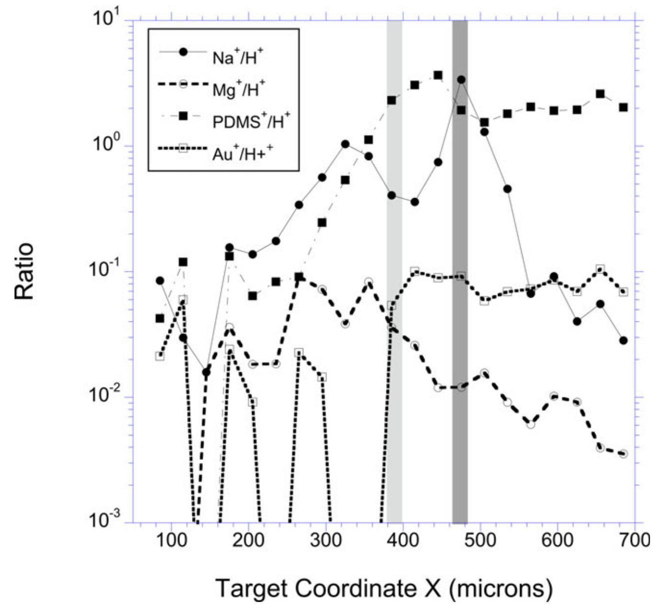

Fig. 8. The ratios to hydrogen of sodium ions (filled circles, solid line), magnesium ions (open circles, thicker dashed line), a fragment of polydimethylsiloxane (PDMS) with mass 73 (filled squares, dashed-dotted line), and gold ions (open squares, thicker dotted line) for particle Roberto Toisvesi.1. The first two species serve as indicators of the presence of a particle, while the second two species indicate the reverse (PDMS is a contaminant that is found on some targets, and the target itself is a gold surface). Sodium is quite high at a single location (indicated by a darker gray bar), but magnesium is low at that same location, and the PDMS and gold are quite high. This may be due to a small particle which lacks magnesium. Another location (indicated by the lighter gray bar) was used as background.

calcium, but no aluminum. Its Ca/Fe ratio is compatible with the CI value. The particle Kathrin shows both Ca and Al; the calcium abundance is also consistent (within errors) with that of CI chondrites, while the Al/Fe ratio is several times that of CI, and could reflect the presence of Al-rich minerals like spinel. Particle Roberto Toisvesi.1 does contain silicon. It also contains calcium and aluminum, but at reduced rather than elevated levels compared to CI, when using the abundances normalized to Si. It does not have any detectable magnesium or iron. Although it is possible that a residual of Si signal from PDMS after background subtraction may have decreased the relative abundances of Ca and Al, there is no basis for assigning a CAI-like composition to this particle.

Particle David Toisvesi.2 shows an absence of silicon, although it is enhanced at two locations in calcium and aluminum. This is consistent with the presence of oxides but not silicates. Silicon-free minerals exist in CAIs, such as spinel ($MgAl_2O_4$), hibonite ($CaAl_{12}O_{19}$), and perovskite ($CaTiO_3$) that are common constituents of CAIs. Less common Ca- and Al-bearing minerals such as grossite ($CaAl_4O_7$) and corundum (Al_2O_3) can also been found in CAIs (MacPherson 2005). No titanium was detectable from particle David Toisvesi.2, arguing against the presence of perovskite. Elemental ratios for Mg, Al, and Ca are Ca/Al = 0.7 and Mg/Ca = 1.8. These numbers first suggest that hibonite ($CaAl_{12}O_{19}$) is probably not present in the analyzed area of David Toisvesi.2, as even a small proportion of hibonite (that has Ca/Al < 0.1) would dramatically decrease the measured Ca/Al ratio. The

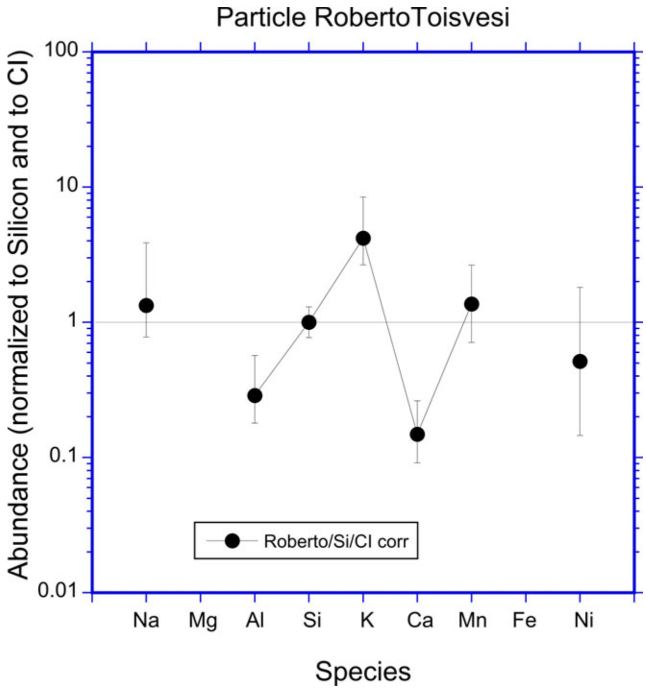

Fig. 9. Abundances of several elements on Roberto Toisvesi.1. The abundance of Na, Al, K, Ca, Mn, and Ni all normalized to Si and to CI chondrites (Lodders 2010). Although calcium and aluminum are present in the particle, they are rather lower than the solar system abundance rather than elevated. Neither magnesium nor iron is present. The value reported for potassium is actually less than 0.1 atom%, but appears to be elevated because the CI value is very low (0.02 atom%). Such Mg-poor and K-rich phases have been identified in Si-rich glasses in Stardust samples (for example Joswiak et al. 2009).

Table 3. Atomic ratios.

	Na/Si	Mg/Si	Al/Si	Ca/Si	Mn/Si	Fe/Si	Ni/Si
Roberto	0.07	0.00	0.02	0.01	0.01	0.00	0.02

same argument pleads for the absence of corundum in David.Toivesi.2. One explanation for such high Ca/Al ratio, associated with no silicon, would be the presence of Ca oxide (CaO), as reported by Greshake et al. (1996) in refractory inclusions from carbonaceous chondrites. They observed that CaO is often encountered as inclusions in spinels, at the submicrometer scale. The elevated Ca/Al elemental ratios measured for David Toivesi.2 could be explained by a mixture of about equal amounts of spinels and Ca oxides. The Mg/Al ratio of 1.8 would require the additional presence of about 20% of periclase (MgO) in the analyzed area. Periclase was relatively rarely observed by Greshake et al. (1996), but always in association with spinels. Another hypothesis to explain the high Ca content of David.Toivesi.2 would be to invoke the presence of calcium carbonate in the particle ($CaCO_3$). Although the presence of carbonates has not been confirmed in comets, carbonates can be formed by nonequilibrium condensation and have been observed in circumstellar environments (e.g., Toppani et al. 2005). The smallest observed CAIs are corundum grains in meteorite matrices (Makide et al. 2009) and only small CAIs (up to a few tens of microns at most) could be contained within the particles that COSIMA observes. The presence of iron and nickel can be explained as the presence of iron-nickel metal (also a high-temperature phase) in close proximity to the CAI, or Fe-Ni sulfide. The fact that only two locations on David show the highest levels of calcium and aluminum argues that the enhancement of these two elements is due to a localized feature (such as a CAI), rather than being a characteristic of the entire dust particle. CaO and periclase observed by Greshake in refractory inclusions from carbonaceous chondrites are interpreted as primary condensates that were embedded with or within the spinels as host minerals. David Toivesi.2 could thus have preserved such primary condensates in the refractory inclusion that has been identified. The sizes of the putative CAIs observed here are in the same size range as those observed in Stardust (Simon et al. 2008; Matzel et al. 2010; Joswiak et al. 2013) and in IDPs (McKeegan 1987) and in micrometeorites.

While the presence of one particle containing minerals consistent with CAIs out of 13 analyzed particles may seem unlikely, in Stardust results on the order of 1% of particles were found to contain CAI minerals (Brownlee and Zolensky, personal communication). The proportion of CAIs in meteorites is also of the order of 1%, as is the proportion of CAIs in micrometeorite samples. This is not so different from that found in this work given the number of particles studied. Consideration of the fraction of beam positions (rather than the number of particles) at which elevated calcium and aluminum were found would result in a fraction even closer to the 1% number cited above. Analysis of more particles will reveal if there is any real discrepancy in the frequency of CAI-like composition between comet 67P/Churyumov–Gerasimenko and comet 81P/Wild 2.

CONCLUSIONS

Thirteen dust particles from Comet 67P/Churyumov–Gerasimenko that were captured by the COSIMA instrument onboard Rosetta were subjected to a compositional analysis using SIMS. Of the 13 particles, one shows compositional evidence (in the form of enhanced levels of calcium and aluminum) of the presence of minerals found in calcium-aluminum-rich inclusions, possibly spinel ($MgAl_2O_4$), CaO, and

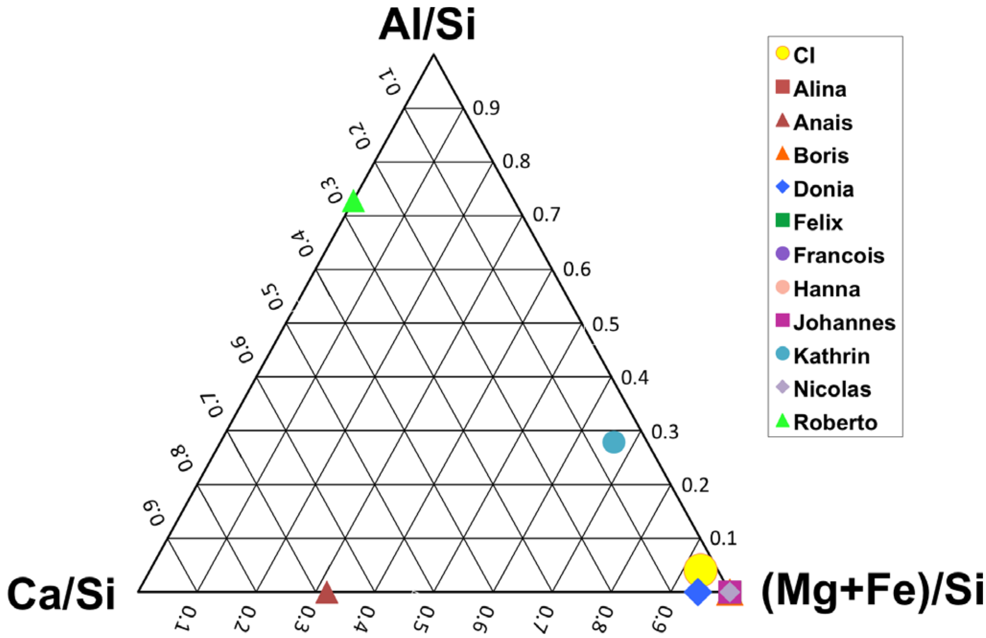

Fig. 10. A ternary diagram for particles from target holder D0. The particles fall into three distinct classes, with Boris, Donia, Felix, Francois, Hanna, Johannes, and Nicolas clustering near the (Mg+Fe)/Si vertex; Anais being richest in calcium but not in aluminum; Kathrin having both calcium and aluminum; and Roberto lying on the calcium-aluminum line. The particle Oscar is not plotted here, as it contained no detectable levels of calcium, magnesium, or aluminum. Particle David is also not plotted as it contains no silicon. Although both particles contain calcium and one contains aluminum, the calcium abundance of Anais and Kathrin agree within errors with that of CI chondrites, i.e., they do not show evidence of CAI-like minerals.

Table 4. Atomic ratios for various particles on target holder D0.

Particle	Na/Fe	Mg/Fe	Al/Fe	Si/Fe	Ca/Fe	Mn/Fe	Ni/Fe
Boris	0.2	0.2	0.0	3.1	0.0	0.0	0.0
Donia	0.5	0.4	0.0	10.7	0.1	0.0	0.0
Kathrin	0.1	0.2	0.6	46.3	0.1	0.7	0.0
Alina	0.9	0.0	0.0	43.5	0.0	0.0	0.0
Anais	0.0	0.0	0.0	0.0	0.0	0.0	0.0
Felix	0.2	0.3	0.0	3.3	0.0	0.0	0.0
Francois	0.3	0.5	0.0	3.2	0.0	0.0	0.0
Hanna	0.3	0.2	0.0	5.7	0.0	0.0	0.0
Johannes	0.3	0.4	0.0	18.1	0.0	0.0	0.0
Nicolas	0.1	0.0	0.0	103.1	0.0	0.0	0.0

periclase (MgO). This particle (denoted as David Toisvesi.2) shows a high enhancement in both calcium and aluminum only on two measured locations out of four. The spectra from this particle contain iron as well, but no silicon. The observed iron is not attributed to the CAIs, and may be due to the presence of iron metal in close proximity to CAIs, or to the presence of Fe sulfides. The remaining 12 particles showed calcium and aluminum consistent with or below the level found in CI chondrites. In nine of the dust particles, there was no detection of either calcium or aluminum, but this may in part be due to an instrumental effect at the time of measurement.

Acknowledgments—COSIMA was built by a consortium led by the Max-Planck-Institut für Extraterrestrische Physik, Garching, Germany in collaboration with Laboratoire de Physique et Chimie de l'Environnement et 8 de l'Espace, Orléans, France; Institut d'Astrophysique Spatiale, CNRS/Université Paris Sud, Orsay, France; Finnish Meteorological Institute, Helsinki, Finland; Universität Wuppertal, Wuppertal, Germany; von Hoerner und Sulger GmbH, Schwetzingen, Germany; Universität der Bundeswehr, Neubiberg, Germany; Institut für Physik, Forschungszentrum Seibersdorf, Seibersdorf, Austria; Institut für Weltraumforschung, Österreichische Akademie der Wissenschaften, Graz, Austria; and is led by the Max-Planck-Institut für Sonnensystemforschung, Göttingen, Germany. The support of the national funding agencies of Germany (DLR, grant 50 QP 1302), France (CNES), Austria, Finland, and the ESA Technical Directorate is gratefully acknowledged. We thank the Rosetta Science Ground Segment at ESAC, the Rosetta Mission Operations Centre at ESOC, and the Rosetta Project at ESTEC for their outstanding work enabling the science return of the Rosetta Mission.

Editorial Handling—Dr. Josep Trigo-Rodríguez

REFERENCES

Bockelee-Morvan D., Gautier D., Hersant F., Hure J. M., and Robert F. 2002. Turbulent radial mixing in the solar nebula as the source of crystalline silicates in comets. *Astronomy & Astrophysics* 284:1107–118.

Brownlee D., Tsou P., Aleon J., Alexander C. M. O., Araki T., Bajt S., Baratta G. A., Bastien R., Bland P., Bleuet P., Borg J., Bradley J. P., Brearley A., Brenker F., Brennan S., Bridges J. C., Browning N. D., Brucato J. R., Bullock E., Burchell M. J., Busemann H., Butterworth A., Chaussidon M., Cheuvront A., Chi M. F., Cintala M. J., Clark B. C., Clemett S. J., Cody G., Colangeli L., Cooper G., Cordier P., Daghlian C., Dai Z. R., D'Hendecourt L., Djouadi Z., Dominguez G., Duxbury T., Dworkin J. P., Ebel D. S., Economou T. E., Fakra S., Fairey S. A. J., Fallon S., Ferrini G., Ferroir T., Fleckenstein H., Floss C., Flynn G., Franchi I. A., Fries M., Gainsforth Z., Gallien J. P., Genge M., Gilles M. K., Gillet P., Gilmour J., Glavin D. P., Gounelle M., Grady M. M., Graham G. A., Grant P. G., Green S. F., Grossemy F., Grossman L., Grossman J. N., Guan Y., Hagiya K., Harvey R., Heck P., Herzog G. F., Hoppe P., Horz F., Huth J., Hutcheon I. D., Ignatyev K., Ishii H., Ito M., Jacob D., Jacobsen C., Jacobsen S., Jones S., Joswiak D., Jurewicz A., Kearsley A. T., Keller L. P., Khodja H., Kilcoyne A. L. D., Kissel J., Krot A., Langenhorst F., Lanzirotti A., Le L., Leshin L. A., Leitner J., Lemelle L., Leroux H., Liu M. C., Luening K., Lyon I., MacPherson G., Marcus M. A., Marhas K., Marty B., Matrajt G., McKeegan K., Meibom A., Mennella V., Messenger K., Messenger S., Mikouchi T., Mostefaoui S., Nakamura T., Nakano T., Newville M., Nittler L. R., Ohnishi I., Ohsumi K., Okudaira K., Papanastassiou D. A., Palma R., Palumbo M. E., Pepin R. O., Perkins D., Perronnet M., Pianetta P., Rao W., Rietmeijer F. J. M., Robert F., Rost D., Rotundi A., Ryan R., Sandford S. A., Schwandt C. S., See T. H., Schlutter D., Sheffield-Parker J., Simionovici A., Simon S., Sitnitsky I., Snead C. J., Spencer M. K., Stadermann F. J., Steele A., Stephan T., Stroud R., Susini J., Sutton S. R., Suzuki Y., Taheri M., Taylor S., Teslich N., Tomeoka K., Tomioka N., Toppani A., Trigo-Rodriguez J. M., Troadec D., Tsuchiyama A., Tuzzolino A. J., Tyliszczak T., Uesugi K., Velbel M., Vellenga J., Vicenzi E., Vincze L., Warren J., Weber I., Weisberg M., Westphal A. J., Wirick S., Wooden D., Wopenka B., Wozniakiewicz P., Wright I., Yabuta H., Yano H., Young E. D., Zare R. N., Zega T., Ziegler K., Zimmerman L., Zinner E., and Zolensky M. 2006. Comet 81P/Wild 2 under a microscope. *Science* 314:1711–1716.

Charnoz S., Aleon J., Chaumard N., Baillie K., and Taillifet E. 2015. Growth of calcium-aluminum-rich inclusions by coagulation and fragmentation in a turbulent protoplanetary disk: Observations and simulations. *Icarus* 252:440–453.

Christophe Michel-Levy M. 1968. Un chondre exceptionnel dans la météorite de Vigarano. *Bulletin Société Français de Minéralogie et de Cristallographie* 91:212–214.

Ciesla F. J. 2007. Outward transport of high-temperature materials around the midplane of the solar nebula. *Science* 318:613–615.

Connelly J. N., Bizzarro M., Krot A. N., Nordlund A., Wielandt D., and Ivanova M. A. 2012. The absolute chronology and thermal processing of solids in the solar protoplanetary disk. *Science* 338:651–655.

Greshake A., Bischoff A., Putnis A., and Palme H. 1996. Corundum, rutile, periclase, and CaO in Ca, Al-rich inclusions from carbonaceous chondrites. *Science* 272:1316–1317.

Hilchenbach M., Kissel J., Langevin Y., Briois C., von Hoerner H., Koch A., Schulz R., Silén J., Altwegg K., Colangeli L., Cottin H., Engrand C., Fischer H., Glasmachers A., Grün E., Haerendel G., Henkel H., Höfner H., Hornung K., Jessberger E. K., Lehto H., Lehto K., Raulin F., RoyL Le, Rynö J., Steiger W., Stephan T., Thirkell L., Thomas R., Torkar K., Varmuza K., Wanczek K.-P., Altobelli N., Baklouti D., Bardyn A., Fray N., Martin P., Ligier N., Lin Z., Merouane S., Orthous-Daunay F.-R., Paquette J., Revillet C., Siljeström S., Stenzel O., and Zaprudin B. 2016. Comet 67P/Churyumov-Gerasimenko: Close-up on dust particle fragments. *The Astrophysical Journal Letters* 816:L32.

Hornung K., Kissel J., Fischer H., Mellado E. M., Kulikov O., Hilchenbach M., Kruger H., Engrand C., Langevin Y., Rossi M., and Krueger F. R. 2014. Collecting cometary dust particles on metal blacks with the COSIMA instrument onboard ROSETTA. *Planetary and Space Science* 103:309–317.

Joswiak D. J., Brownlee D. E., Matrajt G., Westphal A. J., and Snead C. J. 2009. Kosmochloric Ca-rich pyroxenes and FeO-rich olivines (Kool grains) and associated phases in Stardust tracks and chondritic porous interplanetary dust particles: Possible precursors to FeO-rich type II chondrules in ordinary chondrites. *Meteoritics & Planetary Science* 44:1561–1588.

Joswiak D. J., Brownlee D. E., and Matrajt G. 2013. Newly discovered CAI in Comet Wild 2: A refractory inclusion analogous to type C CAI precursors. *Meteoritics & Planetary Science* 48:A194.

Kissel J., Altwegg K., Clark B. C., Colangeli L., Cottin H., Czempiel S., Eibl J., Engrand C., Fehringer H. M., Feuerbacher B., Fomenkovao M., Glasmachers A., Greenberg J. M., Grun E., Haerendel G., Henkel H., Hilchenbach M., Von Hoerner H., Hofner H., Hornung K., Jessberger E. K., Koch A., Kruger H., Langevin Y., Parigger P., Raulin F., Rudenauer F., Ryno J., Schmid E. R., Schulz R., Silen J., Steiger W., Stephan T., Thirkell L., Thomas R., Torkar K., Utterback N. G., Varmuza K., Wanczek K. P., Werther W., and Zscheeg H. 2007. COSIMA—High resolution time-of-flight secondary ion mass spectrometer for the analysis of cometary dust particles onboard Rosetta. *Space Science Reviews* 128:823–867.

Krüger H., Stephan T., Engrand C., Briois C., Siljeström S., Merouane S., Baklouti D., Fischer H., Fray N., Hornung K., Lehto H., Orthous-Daunay F.-R., Rynö J., Schulz R., Silén J., Thirkell L., Trieloff M., and Hilchenbach M. 2015. COSIMA-Rosetta calibration for in situ characterization of 67P/Churyumov–Gerasimenko cometary inorganic compounds. *Planetary and Space Science* 117:35–44.

Langevin Y., Hilchenbach M., Ligier N., Merouane S., Hornung K., Engrand C., Schulz R., Kissel J., Rynö J., Eng P., and the COSIMA team. 2016. Typology of dust particles collected by the **COSIMA** mass spectrometer in the inner coma of 67P/Churyumov-Gerasimenko. *Icarus* 271:76–97.

Levison H. F. and Morbidelli A. 2003. The formation of the Kuiper belt by the outward transport of bodies during Neptune's migration. *Nature* 426:419–421.

Lodders K. 2010. Solar system abundances of the elements. In *Principles and perspectives in geochemistry*, edited by Goswami A. and Reddy B. E. New York: Springer. pp. 379–417.

MacPherson G. J. 2005. Calcium-aluminum-rich inclusions in chondritic meteorites. In *Meteorites, comets and planets*, edited by Davis A. M., Holland H. D., and Turekian K. K. Treatise on Geochemistry. Oxford: Elsevier-Pergamon. pp. 201–246.

Makide K., Nagashima K., Krot A. N., Huss G. R., Hutcheon I. D., and Bischoff A. 2009. Oxygen- and magnesium-isotope compositions of calcium-aluminum-rich inclusions from CR2 carbonaceous chondrites. *Geochimica et Cosmochimica Acta* 73:5018–5050.

Matzel J. E. P., Ishii H. A., Joswiak D., Hutcheon I. D., Bradley J. P., Brownlee D., Weber P. K., Teslich N., Matrajt G., McKeegan K. D., and MacPherson G. J. 2010. Contraints on the formation age of cometary material from the NASA Stardust Mission. *Science* 328:483–486.

McKeegan K. D. 1987. Oxygen isotopes in refractory straospheric dust particles—Proof of extraterrestrial origin. *Science* 237:1468–1471.

Merouane S., Langevin Y., Stenzel O., Altobelli N., Della Corte V., Fischer H., Fulle M., Hornung K., Ligier N., Rotundi A., Ryn̂J., Schulz R., Hilchenbach M., and Kissel J., and COSIMA Team. 2016. Properties of the dust particles in the coma of 67P/Churyumov-Gerasimenko measured in-situ by the COSIMA instrument on board Rosetta. To be published in *Astronomy & Astrophysics*. under revision.

Nakamura T., Tsuchiyama A., Akaki T., Uesugi K., Nakano T., Takeuchi A., Suzuki Y., and Noguchi T. 2008. Bulk mineralogy and three-dimensional structures of individual Stardust particles deduced from synchrotron X-ray diffraction and microtomography analysis. *Meteoritics & Planetary Science* 43:247–359.

Rotundi A., Sierks H., Della Corte V., Fulle M., Gutierrez P. J., Lara L., Barbieri C., Lamy P. L., Rodrigo R., Koschny D., Rickman H., Keller H. U., López-Moreno J. J., Accolla M., Agarwal J., A'Hearn M. F., Altobelli N., Angrilli F., Barucci M. A., Bertaux J.-L., Bertini I., Bodewits D., Bussoletti E., Colangeli L., Cosi M., Cremonese G., Crifo J.-F., Da Deppo V., Davidsson B., Debei S., De Cecco M., Esposito F., Ferrari M., Fornasier S., Giovane F., Gustafson B., Green S. F., Groussin O., Grün E., Güttler C., Herranz M. L., Hviid S. F., Ip W., Ivanovski S., Jerónimo J. M., Jorda L., Knollenberg J., Kramm R., Kührt E., Küppers M., Lazzarin M., Leese M. R., López-Jiménez A. C., Lucarelli F., Lowry S. C., Marzari F., Epifani E. M., McDonnell J. A. M., Mennella V., Michalik H., Molina A., Morales R., Moreno F., Mottola S., Naletto G., Oklay N., Ortiz J. L., Palomba E., Palumbo P., Perrin J.-M., Rodríguez J., Sabau L., Snodgrass C., Sordini R., Thomas N., Tubiana C., Vincent J.-B., Weissman P., Wenzel K.-P., Zakharov V., and Zarnecki J. C. 2015. Dust measurements in the coma of comet 67P/Churyumov-Gerasimenko inbound to the Sun. *Science* 347:aaa3905.

Schmitz S., Brenker F. E., Schoonjans T., Vekemans B., Silversmit G., Vincze L., Burghammer M., and Riekel C. 2009. In situ identification of a CAI candidate in 81P/Wild 2 cometary dust by confocal high resolution synchrotron X-ray fluorescence. *Geochimica et Cosmochimica Acta* 73:5483–5492.

Schulz R., Hilchenbach M., Langevin Y., Kissel J., Silen J., Briois C., Engrand C., Hornung K., Baklouti D., Bardyn A., Cottin H., Fischer H., Fray N., Godard M., Lehto H., Le Roy L., Merouane S., Orthous-Daunay F.-R., Paquette J., Ryno J., Siljestrom S., Stenzel O., Thirkell L., Varmuza K., and Zaprudin B. 2015. Comet 67P/Churyumov-Gerasimenko sheds dust coat accumulated over the past four years. *Nature* 518:216–218.

Shu F. H., Shang H., and Lee T. 1996. Toward an astrophysical theory of chondrites. *Science* 271: 1545–1552.

Simon S. B., Joswiak D. J., Ishii H. A., Bradley J. P., Chi M., Grossman L., Aleon J., Brownlee D. E., Fallon S., Hutcheon I. D., Matrajt G., and McKeegan K. D. 2008. A refractory inclusion returned by Stardust from comet 81P/Wild 2. *Meteoritics & Planetary Science* 43:1861–1877.

Toppani A., Robert F., Libourel G., de Donato P., Barres O., d'Hendecourt L., and Ghanbaja J. 2005. A "dry" condensation origin for circumstellar carbonates. *Nature* 437:1121–1124.

Weisberg M. K., Connolly H. C., and Ebel D. S. 2004. Petrology and origin of amoeboid olivine aggregates in CR chondrites. *Meteoritics & Planetary Science* 39:1741–1753.

Zolensky M. E., Zega T. J., Yano H., Wirick S., Westphal A. J., Weisberg M. K., Weber I., Warren J. L., Velbel M. A., Tsuchiyama A., Tsou P., Toppani A., Tomioka N., Tomeoka K., Teslich N., Taheri M., Susini J., Stroud R., Stephan T., Stadermann F. J., Snead C. J., Simon S. B., Simionovici A., See T. H., Robert F., Rietmeijer F. J. M., Rao W., Perronnet M. C., Papanastassiou D. A., Okudaira K., Ohsumi K., Ohnishi I., Nakamura-Messenger K., Nakamura T., Mostefaoui S., Mikouchi T., Meibom A., Matrajt G., Marcus M. A., Leroux H., Lemelle L., Le L., Lanzirotti A., Langenhorst F., Krot A. N., Keller L. P., Kearsley A. T., Joswiak D., Jacob D., Ishii H., Harvey R., Hagiya K., Grossman L., Grossman J. N., Graham G. A., Gounelle M., Gillet P., Genge M. J., Flynn G., Ferroir T., Fallon S., Ebel D. S., Dai Z. R., Cordier P., Clark B., Chi M. F., Butterworth A. L., Brownlee D. E., Bridges J. C., Brennan S., Brearley A., Bradley J. P., Bleuet P., Bland P. A., and Bastien R. 2006. Mineralogy and petrology of comet 81P/Wild 2 nucleus samples. *Science* 314:1735–1739.